Title

Bruch Membrane Opening Detection Accuracy in Healthy Eyes and Eyes With Glaucoma With and Without Axial High Myopia in an American and Korean Cohort

Authors

Rezapour, Jasmin
Proudfoot, James A
Bowd, Christopher
et al.

Publication Date

2022-05-01

DOI

10.1016/j.ajo.2021.11.030

Peer reviewed

HHS Public Access

Author manuscript

Am J Ophthalmol. Author manuscript; available in PMC 2022 December 15.

Published in final edited form as:

Am J Ophthalmol. 2022 May ; 237: 221–234. doi:10.1016/j.ajo.2021.11.030.

Bruch's membrane opening detection accuracy in healthy and glaucoma eyes with and without axial high myopia in an American and Korean cohort

Jasmin Rezapour[1,2], **James A. Proudfoot**[1], **Christopher Bowd**[1], **Jade Dohleman**[1], **Mark Christopher**[1], **Akram Belghith**[1], **Suzanne M. Vega**[1], **Keri Dirkes**[1], **Min Suh Hee**[3], **Jost B. Jonas**[4,5,6], **Leslie Hyman**[7], **Massimo A. Fazio**[8,9], **Ruti Sella**[1,10,11], **Natalie A Afshari**[1], **Robert N. Weinreb**[1], **Linda M. Zangwill**[1]

[1]Hamilton Glaucoma Center, Shiley Eye Institute, Viterbi Family Department of Ophthalmology, UC San Diego, La Jolla, CA, United States

[2]Department of Ophthalmology, University Medical Center of the Johannes Gutenberg University Mainz, Germany

[3]Department of Ophthalmology, Haeundae Paik Hospital, Inje University College of Medicine, Korea

[4]Department of Ophthalmology, Medical Faculty Mannheim, Ruprecht-Karls-University Heidelberg, Germany

[5]Institute of Molecular and Clinical Ophthalmology Basel, Switzerland

[6]Institute of Clinical and Scientific Ophthalmology and Acupuncture Jonas & Panda, Heidelberg, Germany

[7]Wills Eye Hospital, Thomas Jefferson University, Philadelphia, PA, United States

[8]Department of Ophthalmology and Vision Science, School of Medicine, The University of Alabama at Birmingham, Birmingham, AL, United States

[9]Department of Biomedical Engineering, School of Engineering, The University of Alabama at Birmingham, Birmingham, AL, United States

[10]Department of Ophthalmology, Rabin Medical Center, Petah Tikva, Israel

[11]Sackler Faculty of Medicine, Tel Aviv University, Tel Aviv, Israel

Abstract

[*]Corresponding author: Linda M. Zangwill, 9500 Gilman Drive, La Jolla, CA 92093-0946, Shiley Eye Institute/Hamilton Glaucoma Center, Viterbi Family Department of Ophthalmology, University of California, San Diego, T: (858) 534-7686, lzangwill@health.ucsd.edu.

Disclosures

b) Financial Disclosures

No financial disclosures

Purpose: To determine the predictors of Bruch's membrane opening (BMO) location accuracy and the visibility of the BMO location in glaucoma and healthy individuals with and without axial high myopia.

Design: Cross-sectional study

Methods: Healthy and glaucoma eyes from an American study- and a Korean clinic population were classified into 2 groups; no axial high myopia (axial length (AL) <26mm) and axial high myopia (AL ≥26mm). The accuracy of the automated BMO location on optic nerve head (ONH) Spectralis optical coherence tomography (OCT) radial scans was assessed by expert reviewers.

Results: Four hundred thirty-eight non-highly myopic eyes (263 subjects) and 113 highly myopic eyes (81 subjects) were included. In healthy eyes with and without axial high myopia, 9.1% and 1.7% had indiscernible BMOs while 54.5% and 87.6% were accurately segmented, respectively. 36.4% and 10.7% of eyes with indiscernible BMO's were manually correctable (respectively, p=0.017). In glaucoma eyes with and without high myopia, 15.0% and 3.2% had indiscernible BMOs, 55.0% and 38.2% were manually corrected, and 30.0% and 58.7% were accurately segmented without need for manual correction (respectively, p=0.005). Having axial high myopia, larger AL, larger BMO tilt angle, lower BMO ovality index (more oval), and glaucoma diagnosis were significant predictors of BMO location inaccuracy in multivariable logistic regression analysis.

Conclusions: As BMO location inaccuracy was 2.4 times more likely in eyes with high myopia regardless of diagnosis, OCT images of high myopes should be reviewed carefully and when possible, BMO location should be corrected before using ONH scan results for clinical management of glaucoma.

Background

Early glaucoma detection is of utmost importance to slow down or even stop disease progression in this chronic and potentially vision-threatening disease.[1] Structural loss in the optic nerve head (ONH) is often visible before perimetric visible visual field (VF) defects occur.[2,3] Optical coherence tomography (OCT) enables objective structural loss detection and is the standard of care along with visual field testing for detecting glaucoma and monitoring its progression.

Glaucoma diagnosis based on clinical optic disc examination in (highly) myopic eyes can be difficult due to morphologic changes such as disc tilt and enlarged peripapillary areas which mimics glaucomatous ONH characteristics.[4,5] Structural changes associated with myopia also pose significant challenges to diagnose and monitor glaucoma using OCT. For example, the diagnostic accuracy of peripapillary RNFL measurements in high myopes based on comparison to commercial OCT reference database of healthy non-highly myopic eyes has been shown to be lower due to the temporalization of the location of the RNFL peaks, leading to a misclassification of sectoral values as outside normal limits based on measurements from healthy eyes.[6–8] In addition, a recent study of myopic eyes highlighted the importance of assessing RNFL measurements relative to an anatomically accurate ONH center because sectoral circumpapillary RNFL (cpRNFL) thickness measured at fixed distances from the center of the of the Bruch's membrane opening (BMO) were

significantly different from those measured relative to the center of the clinical disc margin identified on infrared fundus image (i.e. *en face* images).[9] These challenges are compounded by the difficulty in identifying the location of the BMO in highly myopic eyes.

The BMO is an important anatomical feature that is used by OCT instruments to define the ONH center to determine the location of RNFL thickness measurements at predetermined diameters in the circumpapillary retina.[9] RNFL thickness is the primary structural parameter utilized for detecting glaucoma and monitoring its progression. Moreover, the BMO also is used to measure the neuroretinal rim, and BMO-minimum rim width (MRW, defined as the shortest distance between the BMO and the internal limiting membrane; ILM). Diagnostic accuracy for glaucoma detection of the BMO-MRW is reportedly similar or better than that of RNFL thickness and confocal scanning laser ophthalmoscope (CSLO) neuroretinal rim measurements and BMO-MRW change over time has been shown to vary by race.[10–16] BMO location also is used to differentiate between different types of peripapillary atrophy (PPA), as beta- and gamma-PPA, and has been investigated as a biomarker to distinguish between myopia and glaucoma.[17–20]

Correct BMO localization is therefore necessary for appropriate representation of the optic nerve head in OCT scans and is essential for accurate measurement and interpretation of glaucomatous optic nerve and RNFL damage. Identifying the BMO in eyes with high myopia can be challenging[21] due at least in part to the differences in the appearance of the ONH, with highly myopic eyes having a greater degree of tilt and ovality than non-myopic eyes.[22,23] With increasing prevalence of myopia,[24–26] especially in Asian populations[27] and given the fact that myopia is a risk factor for glaucoma,[28–32] it is important to determine the accuracy of BMO detection in highly myopic eyes.

The objective of this study is to estimate the accuracy of OCT-based automated BMO detection and the likelihood of indiscernible BMOs in an American and Korean cohort of healthy and glaucoma subjects with and without high myopia. In addition, anatomical features predictive of location accuracy and indiscernible BMOs are evaluated.

Methods

Glaucoma patients and healthy subjects from the Diagnostic Innovations in Glaucoma Study (DIGS; clinicaltrials.gov identifier NCT00221897) and a Korean clinic population from Haeundae Paik Hospital (Busan, South Korea) were included in this cross-sectional study.

Study methods were approved by the Institutional Review Board (IRB) of the University of California San Diego and adhered to the tenets of the Declaration of Helsinki and the Health Insurance Portability and Accountability Act. Methods also were approved by the IRB of Haeundae Paik Hospital (Busan, South Korea) and a written informed consent of the participants was waived. A detailed description of the DIGS study design has been published elsewhere.[33]

Exclusion criteria:

Participants were excluded if they had a history of intraocular surgery (except for cataract surgery or glaucoma surgery), secondary causes for glaucoma, visual fields due to other ocular or systemic diseases, significant cognitive impairment, inability to perform visual field examinations reliably.[33]

Study subjects were ≥18 years old and had open anterior chamber angles at study entry. All participants underwent a complete ophthalmologic examination including best-corrected visual acuity and refractive error assessment, standard automated perimetry (Humphrey Field Analyzer; 24–2 Swedish interactive thresholding algorithm [SITA]; Carl-Zeiss Meditec), intraocular pressure (IOP) measurement (Goldmann applanation tonometry), gonioscopy, dilated fundus examination, central corneal thickness (CCT) measured with ultrasound pachymetry (DGH Technology, Inc., Exton, PA), coherence interferometry measurement of the axial length (IOLMaster, Carl Zeiss Meditec, Dublin, CA), simultaneous stereophotography of the optic disc and macula spectral-domain-OCT measurement. If spherical equivalent was available only after cataract/refractive surgery we did not include SE in the analysis.

For this report, glaucoma is defined based on photograph-based glaucomatous optic disc damage and the existence of corresponding glaucomatous visual field loss (HFA II with 24–2 testing using the Swedish Interactive Thresholding Algorithm, Carl Zeiss Meditec Inc., Dublin, CA).[33] Glaucomatous optic disc damage was defined as focal or diffuse narrowing of the neuroretinal rim, and/or presence of RNFL defects characteristic of glaucoma on optic disc stereophotographs, diagnosed by two masked trained observers. Glaucomatous VF damage was defined as two repeatable and reliable (<33% fixation losses and false negatives, and <33% false positives) visual field tests with a glaucoma hemifield test (GHT) outside normal limits and/ or a pattern standard deviation (PSD) with a p-value <0.05 with a similar of pattern of defect on consecutive abnormal tests.[33]

Healthy participants had healthy appearing optic discs and RNFL based on masked stereoscopic photograph assessement with no history of repeatable abnormal VF results and no history of elevated intraocular pressure (IOP) (all IOP ≤ 21 mm Hg) in either eye. Normal VFs were defined as those with MD and pattern standard deviation (PSD) with p values > 5% and a Glaucoma Hemifield Test (GHT) result within normal limits.

Due to optic disc changes in highly myopic eyes, optic disc photographs of highly myopic eyes were graded independently by two reviewers (JR and CB) after a training with a senior consultant with extensive expertise in myopia and glaucoma (JBJ). Diagnosis was defined by consensus among the two reviewers and by adjudication by the senior consultant in case of disagreement.

Healthy (non-glaucomatous) and glaucoma eyes in the American and Korean cohorts were classified in two groups by axial length, no axial high myopia (axial length ≤26mm) and axial high myopia (AL >26mm). In this study we defined myopia by axial length, rather than spherical equivalent, as it is known from prior studies that axial elongation can lead to morphological changes in the optic disc region and the fundus and that there is a stronger

correlation between axial elongation and optic disc changes than spherical equivalent and optic disc changes.[4,34] In addition, with this definition, we could more accurately assess myopia status using axial length in eyes after refractive or cataract surgery.

Spectral-domain OCT imaging

The Spectralis OCT (Glaucoma Module Premium Edition, version 6.10; Heidelberg Engineering Inc, Heidelberg, Germany) optic nerve head radial circle (ONH-RC) imaging protocol was used to obtain 24 radial scans and three circle scans centered on the ONH. A total of 24 B-scans averaged 25x using automatic real-time (ART), and a resolution of approximately 6 microns between A-scans (1024 A-scans per B-scan) were captured per eye. The innermost termination of the Bruch's membrane (BM) was automatically identified by the instrument software as the BMO in each of the 24 radial scans. The operator then reviews and confirms or corrects the location of the BMO, and if necessary retakes the scan to improve Bruch's Membrane Opening Centration, the distance between the scan center and the BMO center (ΔBMOC). The scan center was based on 4 BMO locations from 2 B-scans identified by the operator during live image acquisition whereas the BMO center was defined as the center of the BMO contour based on 48 BMO locations defined on the 24 High-resolution B-scans (Supplemental Figure 1). According to the manufacturer recommendations, ΔBMOC should be smaller than 100μm to guarantee comparability of the computed RNFL thickness with the device normative database RNFL thickness measurements (Supplemental Figure 1).[35] In this study, eyes with ΔBMOC > 100 μm were included to reflect clinical practice where it is often difficult to meet the criteria in highly myopic eyes.

For all eyes enrolled in this study, the 48 automatically detected BMO locations obtained were reviewed for accuracy by two reviewers with extensive training and experience in BMO detection in myopic eyes. The first experienced reviewer manually adjusted the BMO location as needed. If the first reviewer had difficulty in identifying the BMO location in more than 4 different B-scans in one eye (4 out of 8 BMO locations, but in 4 different scans), the eye was referred to a second reviewer. The second reviewer evaluated the scans with the primary reviewer in order to reach consensus on the correct BMO location in that eye. If the second reviewer also determined that it was not possible to confidently detect the BMO locations in more than 4 B-scans (more than 4 out of 8 BMO locations in >4 different B-scans) this eye was classified as having indiscernible BMOs.[36] BMO location was classified as follows: (1) Accurate automated BMO location (Figure 1), (2) manually corrected BMO location (Figure 2) and (3) indiscernible BMO (manual correction not possible, Figure 3). BMO was defined as indiscernible only when 2 trained and experienced reviewers could not confidently place the BMO locations in more than 4 B-scans. Scans with low quality (quality score <15) were also excluded.

We also qualitatively evaluated characteristics of the images and b-scans of the 27 eyes with indiscernible BMO. Two graders (JR and SV) reviewed the images and 24 b-scans of each of the 27 eyes with indiscernible BMO and reached consensus on the location of the b-scans and whether there was vessel shadowing or low image quality that influenced the ability to

detect the BMO location. In addition, the enface OCT ONH image was reviewed for the existence and location of PPA.

Optic nerve head measurements

Standard software ONH measurements:

BMO area, BMO-MRW, ΔBMOC and image quality score were measured automatically by the instrument software. Specifically, the BMO-MRW is automatically computed for each radial B-scan. The resultant 48 BMO-MRW measurements (each B-scan contributed 2 BMO locations) were averaged to generate global, temporal, superotempral, superonasal, nasal, inferonasal, inferotemporal MRWs.

Custom Bruch's Membrane Opening Ovality Index, Tilt and Rotation Angle Measurements:

BMO ovality index, BMO tilt angle and BMO rotation angle were calculated using the San Diego Automated Layer Segmentation Algorithm (SALSA) based on the automatic or corrected BMO location.[37,38] All custom computations were performed using three-dimensional (3D) rectangular coordinates. The coordinate transformation of each pixel was determined by the A-scan and B-scan-index, along with the scan center and the fovea-BMO angle provided by the acquisition software. Major and minor axes of a BMO fit ellipse were defined as the longest and shortest axis of the fitted ellipse.

The BMO ovality index was calculated by dividing the minor axis by the major axis.[38] For automated BMO-based tilt assessment, 2 BM boundary (BMB) points on the furthest outward 2 pixels on the BM contour and 2 BMO points were selected. Each BMB and BMO point was transformed into a rectangular coordinate space. One plane was fit to the BMB points and one plane to the BMO points, applying the least-squares method. BMO tilt was defined as the angle between the BMO plane and the BMB plane and computed by assessing the angle between their normal vectors.

In this study we aimed to assess the anatomically accurate 3D morphological characteristics of the optic disc. We therefore applied a new term "BMO rotation"[38,39] instead of the term "optic disc torsion" used in studies that applied optic disc photographs to identify the clinical disc margin.[40] Measurements are based on the BMO, considered to be an anatomically based landmark, which has been shown to be more accurate and reliable than subjective measurements based on the clinical disc margin seen on fundus photographs.[10,36,37] Furthermore the term torsion implies presence of shearing deformations in the ONH tissue, which cannot be confirmed without histological or biomechanical analysis of the tissue. For details of BMO ovality index-, BMO tilt angle- and BMO rotation angle calculations see Rezapour et al.[38]

For calculation of the BMO rotation angle, the center of mass of the BMO points was subtracted from each BMO point and rotated so that the fit plane lay in the xy-plane (i.e., the transverse cross-section of the radial image). These points were projected on a reference plane and used to fit an ellipse in the 2D space of the reference plane. The ellipse was fit using the least square method by optimizing the conic equation of an arbitrary ellipse. Then, the orientation of the ellipse was calculated separately and added to the fit form.

The major axis orientation was reported with reference to the temporal axis (Fovea BMO center). All angles were reported after transforming the vectors used in their computations into physical space by scaling according to the Scale X and Scale Z constants in the image volume metadata. The rotation angle was calculated relative to the Fovea BMO center.

Statistical Analyses

Data are presented as mean (95% confidence interval) and count (percentage) for continuous and categorical variables, respectively. The statistical significance of differences in patient-level characteristics between myopia groups was determined by two-sample t-tests for continuous variables and Fisher's exact test for categorical variables. Eye-level characteristics were compared via generalized estimating equations (GEE), with an exchangeable working correlation assumed to account for within-patient clustering. Rates of location failure by eye classification and myopia were compared using logistic GEE. The influence of different patient and ocular characteristics on the odds of non-accurate location was computed via univariable and multivariable logistic GEE.

Results

A total of 551 eyes (344 subjects) were included in this cross-sectional study; 438 eyes (79.5%) were classified as not-highly myopic (AL≤ 26mm) (263 subjects) and 113 eyes (20.5%) as highly myopic (AL> 26mm) (81 subjects). The 154 healthy eyes included 33 (21.4%) highly myopic eyes while the 397 glaucoma eyes included 80 (20.1%) highly myopic eyes. Demographic information and eye characteristics are presented in Table 1.

Highly myopic individuals were significantly younger ($p<0.001$) and more often of Asian descent ($p<0.001$) than non-highly myopic individuals. There was no significant difference in the proportion of healthy eyes in the highly myopic and non-highly myopic groups (29.2% vs. 27.6%, respectively $p=0.705$). The OCT quality score was slightly higher in highly myopic eyes (30.3 [29.6, 30.9]), compared to non-highly myopic eyes (29.3 [28.9, 29.7], $p=0.010$). The BMO-based ovality index and BMO rotation angle were significantly smaller (more oval) and BMO tilt angle significantly larger in highly myopic eyes compared to non-highly myopic eyes (all $p<0.001$). OCT ΔBMOC was significantly lower in non-highly myopic eyes (49.2 μm (43.9, 54.5)) compared to highly myopic eyes (96.7μm [81.0, 112.5] $p<0.001$).). BMO-MRW was significantly smaller in highly myopic compared to non-highly myopic eyes globally (208.5μm [195.4, 221.5] and 222.4 [213.7, 231.0]), respectively, $p=0.038$), in the temporal-inferior sector (190.6μm [173.0, 208.2], vs 211.9 [200.0, 223.7], respectively, $p=0.023$) and nasal-superior sector (219.3μm [204.0, 234.5], vs 249.5 [239.2, 259.9], respectively $p<0.001$).

The proportion of eyes with accurate BMO location was significantly lower in the highly myopic healthy eyes (18/33 [54.5%]) and glaucoma eyes (24/80 [30.0%]) than non-highly myopic healthy eyes (106/121 [87.6%]) and glaucoma eyes (186/317 [58.7%]) (Table 2). Similarly, the proportion of eyes with indiscernible BMO was significantly higher in highly myopic eyes compared to non-highly myopic eyes in both the healthy (9.1% vs 1.7%, $p=0.017$) and glaucoma eyes (15.0% vs 3.2%, $p=0.005$) (Table 2 and Figure 4). Similar

trends were found when the American and Korean datasets were analyzed separately before pooling the data across sites (data not shown).

Univariable logistic regression analysis and the associated odds ratios (OR) assessing demographic and eye specific predictors associated with BMO location inaccuracy (manually corrected and indiscernible combined) are presented in Table 3. Both longer axial length as a continuous variable and as a categorical variable (high myopia versus not high myopia) were strong predictors of higher BMO location inaccuracy. Specifically, for each 1 mm larger axial length, the odds (95% CI) of BMO location inaccuracy were 1.36 (1.20, 1.54, p<0.001). Eyes with axial high myopia were 3.38 (p<0.001) times more likely to have initial inaccurate BMO location than eyes without axial high myopia. In addition, lower BMO ovality index (OR (95% CI) per 0.1 lower (more oval): 1.57 [1.21, 2.04], p<0.001), larger BMO tilt angle (OR [95% CI] per degree higher): 1.24 [1.14, 1.35], p<0.001), larger BMO area (OR (95% CI) per 1 mm^2 higher: 1.40 [1.03, 1.90], p=0.032) and thinner global BMO-MRW (OR (95% CI) per 10 μm thinner: 1.06 [1.03 109], p<0.001) were associated with location inaccuracy. Other factors associated with a higher univariable odds (OR, [95%]) of location inaccuracy included male sex (1.56 [1.06, 2.31], p=0.025), Asian Descent (2.63 [1.42, 4.88], p=0.002) and worse visual field MD (per 1 dB lower) (1.10 [1.07, 1.13], p<0.001.

Five multivariable models (Table 4) of BMO location error were developed for each of the 5 myopia related parameters (spherical equivalent, axial length, BMO ovality index, BMO tilt angle and high myopia status) that were statistically significant (p<0.05) based on the univariable analysis. The separate multivariable models were developed because the 5 myopia related parameters were highly correlated with one another (data not shown). Glaucoma eyes were more than 4 times likely to have inaccurate location than healthy eyes and highly myopic eyes were 2.4 times more likely to have inaccurate BMO location than non-highly myopic eyes. Moreover, axial length, BMO ovality index, BMO tilt angle, but not spherical equivalent were significant predictors of BMO location inaccuracy. Specifically, the odds (95% CI) of BMO location inaccuracy for each 1 mm larger axial length were 1.20 (1.02, 1.40, p=0.023). Lower BMO ovality index (per 0.1 units lower – more oval) (OR [95% CI]: 1.45 [1.09, 1.93], p=0.010), larger BMO tilt angle (per degree) (OR [95% CI]: 1.18 [1.07, 1.30], p=0.001) and highly myopic eyes (AL> 26mm) (OR [95% CI]: 2.41 [1.36, 4.25], p=0.002) were also associated with BMO location inaccuracy. None of the other parameters that were statistically significant in the univariable analysis were predictors of BMO location inaccuracy in the multivariable analysis.

The qualitative evaluation of characteristics of the images and b-scans of the 27 eyes with indiscernible BMO is presented in Table 5. In general, in highly myopic eyes with indiscernible BMOs, indiscernible BMOs were more often located in the temporal (43.5%) than the nasal sectors (26.3%). Vessel shadowing was visible in a relatively small proportion (21.5% and 30.3%) of b-scans in the high and non-high myopic eyes with indiscernible BMOs, respectively. Moreover, the majority (80%) of the highly myopic eyes with indiscernible BMO had a clinical visible PPA zone. In non-highly myopic eyes, the location of indiscernible eyes was similarly distributed in the temporal (27.1%) and nasal sectors (26.3%), but vessel shadowing was more often in the nasal sectors (72.0%) than the

temporal sector (28.0%). Only 50% of the non-highly myopic eyes had a clinically visible PPA zone. The proportion of scans with indiscernible BMO due to vessel shadowing was higher (30.3%) in non-highly myopic eyes than in highly myopic eyes (21.5%). Only 4 eyes had poor quality OCT images; the proportion of eyes with indiscernible BMO due to low image quality was only 13.3% and 16.7% in the non-highly myopic eyes and highly myopic eyes, respectively.

Discussion

This study assessed the accuracy of OCT BMO location in healthy and glaucoma eyes with and without axial high myopia using Spectralis ONH-RC scans. We found that BMO location inaccuracy (manually corrected and indiscernible BMOs) was significantly higher in eyes with axial high myopia compared to eyes without axial high myopia in both healthy and glaucoma subjects. In addition to longer axial length, we found that a more oval BMO, larger BMO tilt angle, axial high myopia status, as well as having glaucoma were significantly associated with BMO location inaccuracy in multivariable analysis. These results suggest that qualitative review and manual correction of the BMO location is critical to ensure accurate assessment of OCT-based ONH morphology for glaucoma management, especially in eyes with high myopia.

Using OCT-based neuroretinal rim area and BMO-MRW in clinical management to diagnose and monitor glaucoma requires accurate BMO localization as the BMO based disc margin. RNFL measurements also are affected by the accuracy of BMO segmentation. If the BMO center is inaccurately identified in myopic eyes, cpRNFL measurements will not be made in the appropriate location for comparison to internal instrument normative reference databases, which can lead to inaccurate designation of cpRNFL sectors as outside or within normal limits.

The current results are consistent with those of Zheng et al[21] who reported a higher proportion of indiscernible BMOs in 1 or more meridian in eyes with high myopia (≥26mm) compared to eyes without high myopia in both glaucoma eyes (32.1% and 8.2%, respectively) and healthy eyes (28.0% and 3.9%, respectively). The authors suggested that the area of beta parapapillary atrophy (PPA) increases with the severity of glaucoma and that the BMO can be indiscernible when the interface between the BM and choroid layer becomes indistinct. This is often the case in eyes with beta PPA, where the retinal pigment epithelium, the choriocapillaris and choroidal vessels are atrophic.[21] The proportion of indiscernible BMOs was lower in the current study than in the study of Zheng et al. in part because we classified eyes as indiscernible when the BMO was indiscernible in 4 or more meridians compared to 1 or more meridians in their study. In addition, we found that the BMO was more often indiscernible due to morphology, and not because of vessel shadowing or image quality in both, highly and non-highly myopic eyes. Moreover, indiscernible BMO locations were more often located in the temporal sectors in the highly myopic eyes, which might be in part due to the higher BMO tilt angle and/or PPA in the temporal sector. These findings are of particular interest in glaucoma diagnostics, as the temporal ONH region corresponds with the central visual field.[41] The results concur with Zheng et al., where the temporal meridian was the most frequent location with indiscernible BMO.[21]

In addition to its importance for using OCT ONH scans for clinical management, accurate BMO localization is critical for investigators actively developing new OCT BMO based parameters to characterize 3D ONH morphology. For example, the neural canal's anatomy can be characterized by assessing the anatomic tilt- and rotation angle of the anterior scleral canal opening relative to a BMO reference plane instead of characterizing ovality or tilt based optic disc photographs.[39,42] For example, by analysing the ONH anatomy using OCT BMO based-morphology, Burgoyne et al. were able to objectively characterize neural canal obliqueness by determining the magnitude and direction of the offset of anterior scleral canal opening relative to BMO.[42] In summary, accurate BMO localization is not only critical for appropriate interpretation of OCT ONH scans and cpRNFL thickness in clinical management but also for research characterizing optic disc morphology. For the above mentioned reasons, it is important to understand the challenges in identifying the BMO in highly myopic eyes.

The reasons for incorrect BMO localization by the standard OCT software are likely in part due to the anatomic differences in highly myopic eyes compared to non-highly myopic eyes[42] and because the segmentation algorithms were not developed on highly myopic eyes. However, it should also be noted that the software's BMO localization relies on the manual BMO localization conducted by the operator. If this first step is not done correctly (due to lack of expertise in high myopic eyes) the final BMO localizations provided by the software are inaccurate. Our preliminary results suggest that BMO location accuracy in highly myopic eyes can be improved by using deep learning retinal layer segmentation strategies trained on highly myopic eyes (Belghith, personal communication May 10, 2021). Future improvements in instrument retinal layer segmentation will therefore likely reduce the impact of these BMO segmentation issues.

There are several strengths of this study. First we included two study populations from two different countries providing evidence that indiscernible BMOs in highly myopic eyes are independent of race and that race is not a predictor of location accuracy. We found no differences in the proportion of indiscernible or inaccurate BMO location between the American and Korean populations (data not shown). We also included new OCT parameters that characterize highly myopic discs, BMO based on ovality index, tilt and rotation angle which have not been reported previously. In addition, high myopia was defined in this study by axial length, rather than spherical equivalent used in most studies. By using axial length, we can better predict anatomic differences in the ONH due to axial elongation and include axially elongated eyes without relying on spherical equivalent which changes after refractive and cataract surgery. Furthermore, multivariable models indicated that axial length (and parameters correlated to it) were associated with location inaccuracy, whereas spherical equivalent was not.

Our study has several limitations. First, we included only Spectralis OCT for imaging the optic disc and BMO location and did not directly determine the frequency of accurate BMO detection in other OCT instruments. However, the accuracy of BMO detection also is relevant to other OCT instruments, including Cirrus (Carl Zeiss Meditec, Dublin, CA), AngioVue/RTVue (Optovue Inc, Fremont CA) and the swept source DRI and Maestro Topcon (Tokyo, Japan) OCT. These instruments rely on the identification of the innermost

segment of the Bruch's membrane or the Bruch's membrane/ retinal pigment epithelium complex for calculation of ONH parameters and cpRNFL thickness at a fixed distance from the center of the BMO. In addition, not all OCT images were reviewed by both reviewers. All highly myopic eyes were reviewed by both reviewers, but non-highly myopic eyes were only assessed by 2 reviewers if the first reviewer was not able to manually correct the BMO localization in more than 4 different OCT B-scans. However, extensive training and review of eyes with difficult BMO detection (both with and without axial high myopia) was completed by both reviewers, which facilitated consensus even in the most challenging eyes. Finally, we did not exclude poor quality scans or scans in which the manufacturer's recommended distance between the BMO center of the ONH-RC scans and the center of the image (ΔBMOC) was not met. We included all acquired scans to better reflect clinical practice as it can be challenging to acquire images of highly myopic eyes that meet general quality and BMOC distance requirements. Although a significantly larger BMO/ scan center distance was found in highly myopic eyes, it was a predictor for localization failure in univariate but not multivariable analysis.

In conclusion, we found highly myopic eyes are significantly more likely to have inaccurate BMO locations and indiscernible BMOs in both healthy and glaucoma eyes than non-highly myopic eyes. In addition, we found that axial length and parameters that are associated with high myopia such as a more oval BMO configuration (smaller BMO ovality index) and higher BMO tilt angle were predictors of BMO localization inaccuracy. Moreover, we found that eyes with glaucoma were over 4 times more likely to have inaccurate BMO locations than healthy eyes. Accurate BMO locations are important for calculating ONH parameters that are used for glaucoma management. For this reason, BMO localization of OCT scans should be reviewed carefully, particularly in highly myopic eyes and if possible manually corrected to ensure accuracy of ONH parameters used in glaucoma management. Promising work to improve BMO localization in highly myopic eyes using deep learning strategies is underway which may alleviate some of the issues.

Supplementary Material

Refer to Web version on PubMed Central for supplementary material.

Acknowledgements

a) Funding / Support

JR: Research Fellowship Grant of the German Research Foundation (DFG) (Grant Nr: RE 4155/1-1) and German Ophthalmological Society (DOG) Grant

JAP: None

CB: None

JD: None

MC: None

AB: None

SMV: None

KD: None

MSH: None

JBJ: None

LH: None

MAF: NEI/NIH, R01EY026574, African Descent and Glaucoma Evaluation (ADAGEs) IV: Alterations of the lamina cribrosa in progression)

RS: None

NAA: None

RNW: Aerie Pharmaceuticals, Allergan, Eyenovia, Implantdata, Unity (consultant); Heidelberg Engineering, Carl Zeiss Meditec, Centervue, Bausch & Lomb, Genentech, Konan Medical, National Eye Institute, Optos, Optovue, Research to Prevent Blindness (research support)

LMZ: Carl Zeiss Meditec, Heidelberg Engineering, National Eye Institute, Optovue, Topcon Medical System Inc. (research support)

Financial Support:

DIGS: EY011008, EY019869, EY014267, EY027510, EY026574, EY029058, P30EY022589; UCSD School of Medicine Summer Research Fellowship; and participant retention incentive grants in the form of glaucoma medication at no cost from Novartis/Alcon Laboratories Inc, Allergan, Akorn, and Pfizer Inc. An Unrestricted grant from Research to Prevent Blindness (New York, NY).

References

1. Resnikoff S, Pascolini D, Etya'ale D, et al. Global data on visual impairment in the year 2002. Bull World Health Organ Nov 2004;82(11):844–51. doi:/S0042-96862004001100009 [PubMed: 15640920]
2. Harwerth RS, Carter-Dawson L, Smith EL 3rd, Barnes G, Holt WF, Crawford ML. Neural losses correlated with visual losses in clinical perimetry. Invest Ophthalmol Vis Sci Sep 2004;45(9):3152–60. doi:10.1167/iovs.04-0227 [PubMed: 15326134]
3. Gordon MO, Kass MA. What We Have Learned From the Ocular Hypertension Treatment Study. Am J Ophthalmol May 2018;189:xxiv–xxvii. doi:10.1016/j.ajo.2018.02.016 [PubMed: 29501371]
4. Marcus MW, de Vries MM, Junoy Montolio FG, Jansonius NM. Myopia as a risk factor for open-angle glaucoma: a systematic review and meta-analysis. Ophthalmology Oct 2011;118(10):1989–1994 e2. doi:10.1016/j.ophtha.2011.03.012 [PubMed: 21684603]
5. Jonas JB, Gusek GC, Naumann GO. Optic disk morphometry in high myopia. Graefes Arch Clin Exp Ophthalmol 1988;226(6):587–90. doi:10.1007/BF02169209 [PubMed: 3209086]
6. Leung CK, Mohamed S, Leung KS, et al. Retinal nerve fiber layer measurements in myopia: An optical coherence tomography study. Invest Ophthalmol Vis Sci Dec 2006;47(12):5171–6. doi:10.1167/iovs.06-0545 [PubMed: 17122099]
7. Leung CK, Yu M, Weinreb RN, et al. Retinal nerve fiber layer imaging with spectral-domain optical coherence tomography: interpreting the RNFL maps in healthy myopic eyes. Invest Ophthalmol Vis Sci Oct 17 2012;53(11):7194–200. doi:10.1167/iovs.12-9726 [PubMed: 22997288]
8. Kang SH, Hong SW, Im SK, Lee SH, Ahn MD. Effect of myopia on the thickness of the retinal nerve fiber layer measured by Cirrus HD optical coherence tomography. Invest Ophthalmol Vis Sci Aug 2010;51(8):4075–83. doi:10.1167/iovs.09-4737 [PubMed: 20237247]
9. Sawada Y, Araie M, Shibata H, Ishikawa M, Iwata T, Yoshitomi T. Differences in Retinal Nerve Fiber Layer Thickness as Assessed on the Disc Center and Bruch's Membrane Opening Center in Myopic Eyes. Ophthalmol Glaucoma May-Jun 2019;2(3):145–155. doi:10.1016/j.ogla.2019.02.008 [PubMed: 32672582]
10. Chauhan BC, O'Leary N, AlMobarak FA, et al. Enhanced detection of open-angle glaucoma with an anatomically accurate optical coherence tomography-derived neuroretinal

rim parameter. Ophthalmology Mar 2013;120(3):535–543. doi:10.1016/j.ophtha.2012.09.055 [PubMed: 23265804]

11. Danthurebandara VM, Sharpe GP, Hutchison DM, et al. Enhanced structure-function relationship in glaucoma with an anatomically and geometrically accurate neuroretinal rim measurement. Invest Ophthalmol Vis Sci Dec 11 2014;56(1):98–105. doi:10.1167/iovs.14-15375 [PubMed: 25503459]
12. Toshev AP, Lamparter J, Pfeiffer N, Hoffmann EM. Bruch's Membrane Opening-Minimum Rim Width Assessment With Spectral-Domain Optical Coherence Tomography Performs Better Than Confocal Scanning Laser Ophthalmoscopy in Discriminating Early Glaucoma Patients From Control Subjects. J Glaucoma Jan 2017;26(1):27–33. doi:10.1097/ijg.0000000000000532 [PubMed: 27636592]
13. Gardiner SK, Boey PY, Yang H, Fortune B, Burgoyne CF, Demirel S. Structural Measurements for Monitoring Change in Glaucoma: Comparing Retinal Nerve Fiber Layer Thickness With Minimum Rim Width and Area. Invest Ophthalmol Vis Sci Oct 2015;56(11):6886–91. doi:10.1167/iovs.15-16701 [PubMed: 26501416]
14. Nakanishi H, Suda K, Yoshikawa M, et al. Association of Bruch's membrane opening and optic disc morphology to axial length and visual field defects in eyes with primary open-angle glaucoma. Graefes Arch Clin Exp Ophthalmol Mar 2018;256(3):599–610. doi:10.1007/s00417-017-3874-8 [PubMed: 29305731]
15. Wu Z, Vianna JR, Reis ASC, et al. Qualitative evaluation of neuroretinal rim and retinal nerve fibre layer on optical coherence tomography to detect glaucomatous damage. Br J Ophthalmol Jul 2020;104(7):980–984. doi:10.1136/bjophthalmol-2019-314611 [PubMed: 31662310]
16. Bowd C, Zangwill LM, Weinreb RN, et al. Racial Differences in Rate of Change of Spectral-Domain Optical Coherence Tomography-Measured Minimum Rim Width and Retinal Nerve Fiber Layer Thickness. Am J Ophthalmol Dec 2018;196:154–164. doi:10.1016/j.ajo.2018.08.050 [PubMed: 30195890]
17. Dai Y, Jonas JB, Huang H, Wang M, Sun X. Microstructure of parapapillary atrophy: beta zone and gamma zone. Invest Ophthalmol Vis Sci Mar 19 2013;54(3):2013–8. doi:10.1167/iovs.12-11255 [PubMed: 23462744]
18. Jonas JB, Wang YX, Zhang Q, et al. Parapapillary Gamma Zone and Axial Elongation-Associated Optic Disc Rotation: The Beijing Eye Study. Invest Ophthalmol Vis Sci Feb 2016;57(2):396–402. doi:10.1167/iovs.15-18263 [PubMed: 26842757]
19. Manalastas PIC, Belghith A, Weinreb RN, et al. Automated Beta Zone Parapapillary Area Measurement to Differentiate Between Healthy and Glaucoma Eyes. Am J Ophthalmol Jul 2018;191:140–148. doi:10.1016/j.ajo.2018.04.021 [PubMed: 29750949]
20. Vianna JR, Malik R, Danthurebandara VM, et al. Beta and Gamma Peripapillary Atrophy in Myopic Eyes With and Without Glaucoma. Invest Ophthalmol Vis Sci Jun 1 2016;57(7):3103–11. doi:10.1167/iovs.16-19646 [PubMed: 27294804]
21. Zheng F, Wu Z, Leung CKS. Detection of Bruch's Membrane Opening in Healthy Individuals and Glaucoma Patients with and without High Myopia. Ophthalmology Oct 2018;125(10):1537–1546. doi:10.1016/j.ophtha.2018.04.031 [PubMed: 29934269]
22. Zhao XJ, Jiang HY, Li YH, et al. Correlations between the optic nerve head morphology and ocular biometrics in highly myopic eyes. Int J Ophthalmol 2018;11(6):997–1001. doi:10.18240/ijo.2018.06.17 [PubMed: 29977814]
23. Hosseini H, Nassiri N, Azarbod P, et al. Measurement of the optic disc vertical tilt angle with spectral-domain optical coherence tomography and influencing factors. Am J Ophthalmol Oct 2013;156(4):737–44. doi:10.1016/j.ajo.2013.05.036 [PubMed: 23891337]
24. Institute BHV. Vision for All to See. Report on the state of eye health and vision care Sydney, Australia. 2013;
25. Dunaway D BI. Worldwide distribution of visual refractive errors and what to expect at a particular location. InFOCUS Center for Primary Eye Care Development 2007;
26. Marsh-Tootle WL, Harb E, Hou W, et al. Optic Nerve Tilt, Crescent, Ovality, and Torsion in a Multi-Ethnic Cohort of Young Adults With and Without Myopia. Invest Ophthalmol Vis Sci Jun 1 2017;58(7):3158–3171. doi:10.1167/iovs.16-20860 [PubMed: 28654981]

27. Fredrick DR. Myopia. Bmj May 18 2002;324(7347):1195–9. [PubMed: 12016188]
28. Quigley HA. Open-angle glaucoma. N Engl J Med Apr 15 1993;328(15):1097–106. doi:10.1056/nejm199304153281507 [PubMed: 8455668]
29. Jonas JB, Budde WM. Optic nerve damage in highly myopic eyes with chronic open-angle glaucoma. Eur J Ophthalmol Jan-Feb 2005;15(1):41–7. [PubMed: 15751238]
30. David R, Zangwill L, Stone D, Yassur Y. Epidemiology of intraocular pressure in a population screened for glaucoma. Br J Ophthalmol Oct 1987;71(10):766–71. [PubMed: 3676147]
31. Wilson MR, Hertzmark E, Walker AM, Childs-Shaw K, Epstein DL. A case-control study of risk factors in open angle glaucoma. Arch Ophthalmol Aug 1987;105(8):1066–71. [PubMed: 3632414]
32. Leske MC, Connell AM, Wu SY, Hyman LG, Schachat AP. Risk factors for open-angle glaucoma. The Barbados Eye Study. Arch Ophthalmol Jul 1995;113(7):918–24. [PubMed: 7605285]
33. Sample PA, Girkin CA, Zangwill LM, et al. The African Descent and Glaucoma Evaluation Study (ADAGES): design and baseline data. Arch Ophthalmol Sep 2009;127(9):1136–45. doi:10.1001/archophthalmol.2009.187 [PubMed: 19752422]
34. Wang Y, Xu L, Zhang L, Yang H, Ma Y, Jonas JB. Optic disc size in a population based study in northern China: the Beijing Eye Study. Br J Ophthalmol Mar 2006;90(3):353–6. doi:10.1136/bjo.2005.081521 [PubMed: 16488961]
35. Heidelberg Engineering. Spectralis Training Guide. Software Manual 2014;
36. Sung MS, Heo MY, Heo H, Park SW. Bruch's membrane opening enlargement and its implication on the myopic optic nerve head. Sci Rep Dec 20 2019;9(1):19564. doi:10.1038/s41598-019-55926-w [PubMed: 31863084]
37. Belghith A, Bowd C, Medeiros FA, et al. Does the Location of Bruch's Membrane Opening Change Over Time? Longitudinal Analysis Using San Diego Automated Layer Segmentation Algorithm (SALSA). Invest Ophthalmol Vis Sci Feb 2016;57(2):675–82. doi:10.1167/iovs.15-17671 [PubMed: 26906156]
38. Rezapour J, Bowd C, Dohleman J, et al. The influence of axial myopia on optic disc characteristics of glaucoma eyes. Sci Rep Apr 23 2021;11(1):8854. doi:10.1038/s41598-021-88406-1 [PubMed: 33893383]
39. Wang YX, Yang H, Luo H, et al. Peripapillary Scleral Bowing Increases with Age and is Inversely Associated with Peripapillary Choroidal Thickness in Healthy Eyes. Am J Ophthalmol Apr 13 2020;doi:10.1016/j.ajo.2020.03.050
40. How AC, Tan GS, Chan YH, et al. Population prevalence of tilted and torted optic discs among an adult Chinese population in Singapore: the Tanjong Pagar Study. Arch Ophthalmol Jul 2009;127(7):894–9. doi:10.1001/archophthalmol.2009.134 [PubMed: 19597111]
41. . Garway-Heath DF, Poinoosawmy D, Fitzke FW, Hitchings RA. Mapping the visual field to the optic disc in normal tension glaucoma eyes. Ophthalmology Oct 2000;107(10):1809–15. doi:10.1016/s0161-6420(00)00284-0 [PubMed: 11013178]
42. Jeoung JW, Yang H, Gardiner S, et al. Optical Coherence Tomography Optic Nerve Head Morphology in Myopia I: Implications of Anterior Scleral Canal Opening Versus Bruch Membrane Opening Offset. Am J Ophthalmol Oct 2020;218:105–119. doi:10.1016/j.ajo.2020.05.015 [PubMed: 32445702]

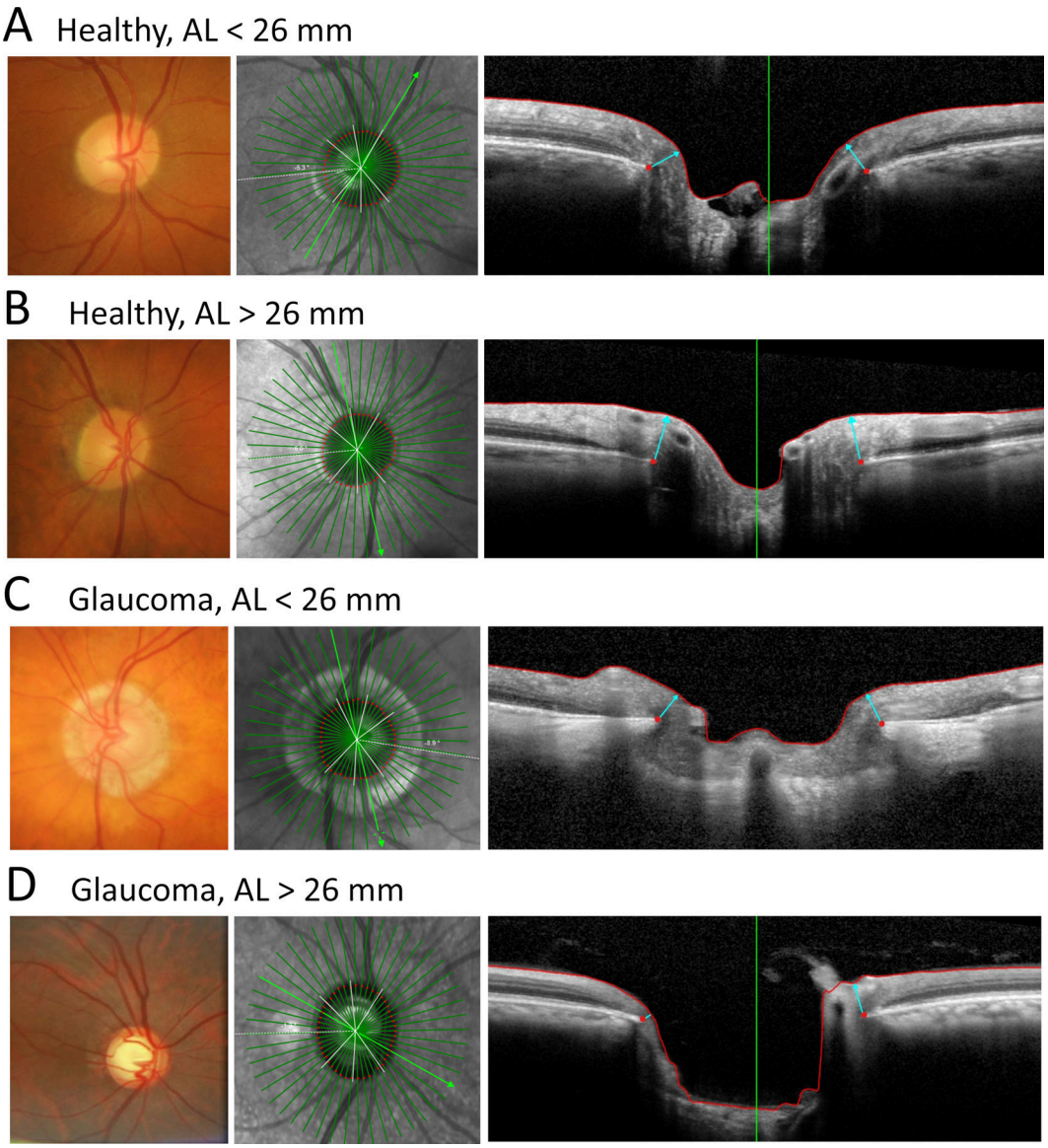

Figure 1.

Automatically accurate BMO location in A) a healthy non-highly myopic eye (AL=23.4mm) B) a healthy highly myopic eye (AL=26.1mm) C) a glaucoma non-highly myopic eye (AL=24.6mm) and D) a glaucoma highly myopic eye (AL=26.2mm)

The image on the left presents a clinical photograph of the optic nerve head, the image in the middle an enface image of the OCT scan and the image on the right a radial B-scan of the OCT scan. The red dots illustrate the automatic correct BMO location, the red line the ILM segmentation and the blue arrows the BMO-MRW.

Abbreviations: AL; axial length, BMO; Bruch's membrane opening, MRW; minimum rim width, OCT; optical coherence tomography

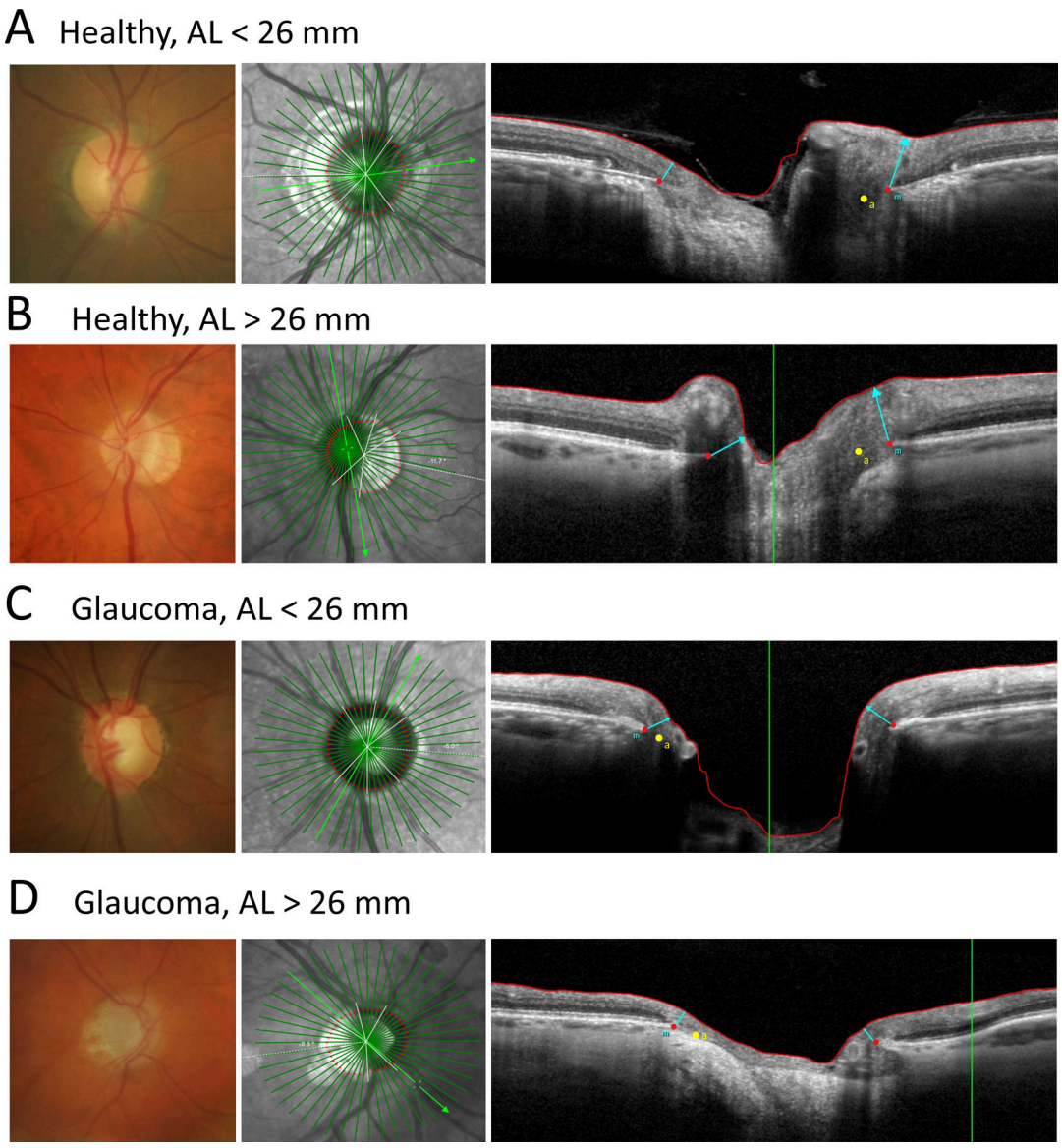

Figure 2.

Manually corrected BMO location (red dot) in A) a healthy non-highly myopic eye (AL=23.8mm) B) a healthy highly myopic eye (AL=27.2mm) C) a glaucoma non-highly myopic eye (AL=23.3mm) and D) a glaucoma highly myopic eye (AL=27.5mm). The image on the left presents a clinical photograph of the optic nerve head, the image in the middle an enface image of the OCT scan and the image on the right a radial B-scan of the OCT scan. The red dots illustrate the correct BMO location, the blue “m” stands for manually corrected, the yellow dots marked with an “a” illustrate the automatic inaccurate BMO location, the red line illustrates the ILM segmentation and the blue arrows the BMO-MRW. Abbreviations: AL; axial length, BMO; Bruch’s membrane opening, MRW; minimum rim width, OCT; optical coherence tomography

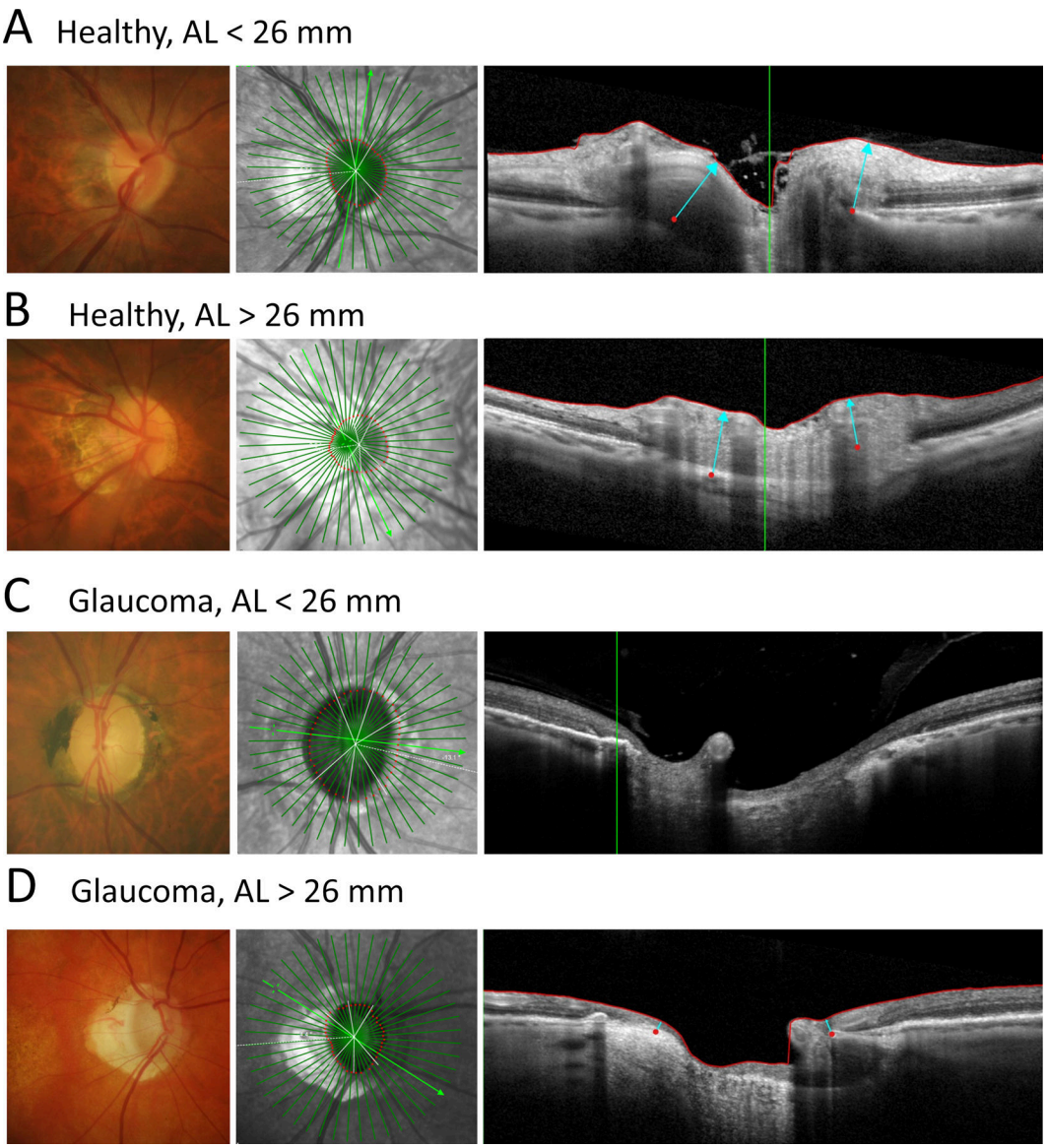

Figure 3.

Indiscernible BMO in A) a healthy non-highly myopic eye (AL=25.5mm) B) a healthy highly myopic eye (29.1mm) C) a glaucoma non-highly myopic eye and (AL=23.6mm) D) a glaucoma highly myopic eye (AL=27.2mm).

The image on the left presents a clinical photograph of the optic nerve head, the image in the middle an enface image of the OCT scan and the image on the right a radial B-scan of the OCT scan. The red dots illustrate the correct and incorrect automatically detected BMO locations. Incorrect BMO locations could not be manually corrected, the red line the ILM segmentation and the blue arrows the BMO-MRW. In Figure 3C the software did not provide automatic BMO locations in some scans, as in the illustrated example.

Abbreviations: AL; axial length, BMO; Bruch's membrane opening, MRW; minimum rim width, OCT; optical coherence tomography

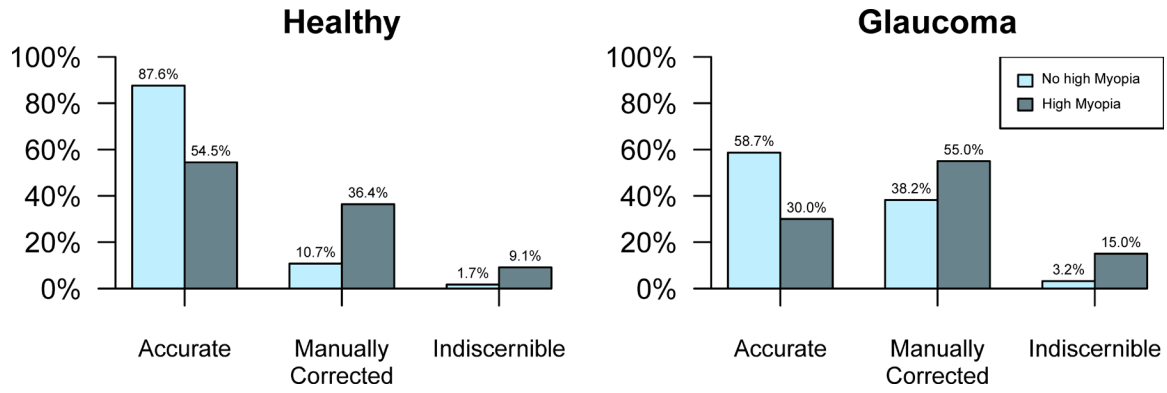

Figure 4.

Percentage of automatic accurate, manually corrected and indiscernible BMO in healthy eyes (left) and glaucoma eyes (right). No high myopia" is defined as axial length ≤26mm and high myopia as axial length >26mm.

Abbreviations: BMO; Bruch's membrane opening

Table 1:

Patient and eye characteristics by axial myopia group in San Diego and Korean eyes.

	Axial Length ≤ 26mm (not-high myopic) (n = 263, 438 Eyes)	Axial Length > 26mm (high myopic) (n = 81, 113 Eyes)	Overall (n = 344, 551 Eyes)	p-value
Patient Characteristics				
Age (years)	69.2 (67.5, 70.9)	58.0 (54.6, 61.4)	66.6 (64.9, 68.2)	**<0.001**
Sex (% Female)	54.8%	42.0%	51.7%	
Race (n, %)				
African Descent	62 (23.6%)	6 (7.4%)	68 (19.8%)	**<0.001**
Asian Descent	38 (14.4%)	41 (50.6%)	79 (23.0%)	
European Descent	156 (59.3%)	32 (39.5%)	188 (54.7%)	
Other / Not Reported	7 (2.7%)	2 (2.5%)	9 (2.6%)	
Eye Characteristics				
[a] **Spherical Equivalent (D)**	−0.91 (−1.17, −0.65)	−4.23 (−5.08, −3.38)	−1.51 (−1.85, −1.17)	**<0.001**
[b] **Visual Field MD (dB)**	−5.69 (−6.44, −4.95)	−7.16 (−8.74, −5.57)	−5.98 (−6.70, −5.27)	0.083
[a] **IOP (mmHg)**	13.5 (13.1, 14.0)	13.2 (12.2, 14.2)	13.5 (13.0, 13.9)	0.563
Axial Length (mm)	24.2 (24.1, 24.3)	26.9 (26.6, 27.2)	24.8 (24.6, 25.0)	**<0.001**
[c] **CCT (μm)**	536.0 (531.2, 540.8)	536.0 (527.6, 544.4)	536.0 (531.5, 540.5)	0.999
[d] **BMO Ovality Index**	0.88 (0.87, 0.89)	0.84 (0.81, 0.86)	0.87 (0.86, 0.88)	**0.001**
[e] **BMO Rotation Angle (°)**	34.3 (32.1, 36.5)	24.2 (18.6, 29.7)	32.3 (30.1, 34.5)	**<0.001**
[d] **BMO Tilt Angle (°)**	2.0 (1.8, 2.2)	4.8 (3.9, 5.6)	2.6 (2.3, 2.8)	**<0.001**
BMO Area (mm^2)	2.13 (2.07, 2.20)	2.30 (2.12, 2.49)	2.17 (2.10, 2.23)	0.084
ΔBMOC (μm)	49.2 (43.9, 54.5)	96.7 (81.0, 112.5)	59.2 (53.4, 65.0)	**<0.001**
OCT Quality Score	29.3 (28.9, 29.7)	30.3 (29.6, 30.9)	29.5 (29.1, 29.8)	**0.010**
Eye Diagnosis				
Healthy	121 (27.6%)	33 (29.2%)	154 (27.9%)	0.705
Glaucoma	317 (72.4%)	80 (70.8%)	397 (72.1%)	
[f] **Global MRW (μm)**	222.4 (213.7, 231.0)	208.5 (195.4, 221.5)	219.4 (211.3, 227.6)	**0.038**
[f] **Temporal MRW (μm)**	169.0 (162.2, 175.9)	168.5 (156.7, 180.3)	168.9 (162.6, 175.2)	0.932
[f] **TS MRW (μm)**	202.1 (192.0, 212.3)	198.5 (182.6, 214.4)	201.4 (192.0, 210.7)	0.674
TI MRW (μm)	211.9 (200.0, 223.7)	190.6 (173.0, 208.2)	207.4 (196.4, 218.3)	**0.023**
Nasal MRW (μm)	254.1 (243.5, 264.6)	238.4 (220.3, 256.5)	250.7 (241.2, 260.2)	0.130
NS MRW (μm)	249.5 (239.2, 259.9)	219.3 (204.0, 234.5)	243.1 (233.3, 252.9)	**<0.001**
NI MRW (μm)	261.2 (248.4, 274.0)	238.9 (216.7, 261.0)	256.5 (245.1, 267.8)	0.084

Data is presented as mean (95% CI) for continuous variables and count (percentage) for categorical variables. Significance is determined by a two-sample t-test and Fisher's exact rest for continuous and categorical patient level variables and generalized estimating equations for eye level variables. Abbreviations: BMO, Bruch's membrane opening; CCT, central corneal thickness; ΔBMOC (μm), distance between the scan center and the BMO center; IOP, intraocular pressure; MD, mean deviation; MRW, minimum rim width; NI, nasal inferior; NS, nasal superior, OCT, optical coherence tomography; SE, spherical equivalent; TI, temporal inferior; TS, temporal superior

Missing 74[a], 19[b], 29[c], 67[d], 69[e], and 1[f] values.

Table 2:

Rates of Location accuracy by diagnosis and axial myopia status in San Diego and Korean eyes.

	Healthy			Glaucoma		
BMO Localization Status	**Non-High Myopia (AL ≤ 26mm) (n = 121)**	**High Myopia (AL > 26mm) (n = 33)**	**p-value**	**Non-High Myopia (AL ≤ 26mm) (n = 317)**	**High Myopia (AL > 26mm) (n = 80)**	**p-value**
Accurate automated	106 (87.6%)	18 (54.5%)	**0.017**	186 (58.7%)	24 (30.0%)	**0.005**
Manually Corrected	13 (10.7%)	12 (36.4%)		121 (38.2%)	44 (55.0%)	
Indiscernible	2 (1.7%)	3 (9.1%)		10 (3.2%)	12 (15.0%)	

Axial length ≤26mm is defined as axial non-high myopia and axial length >26mm as axial high-myopia

Data is presented as count (percentage).

Significance is determined by logistic generalized estimating equations to adjust for both eyes of the patient in the analysis

Abbreviations: AL, axial length

Table 3:

Patient and eye characteristics by BMO location status in San Diego and Korean eyes. Odds ratios (OR) indicate the odds of inaccurate locations.

	BMO Location Status			Univariable Analysis		
	Accurate automated (n = 334)	**Manually Corrected (n = 190)**	**Indiscernible (n = 27)**	**OR Units**	**Inaccurate BMO Location OR (95% CI)**	**p-value**
Age (years)	66.3 (64.7, 67.9)	67.0 (65.4, 68.6)	66.8 (65.2, 68.4)	per year older	0.99 (0.98, 1.01)	0.362
Sex (n, %)						
Female	191 (57.2%)	89 (46.8%)	11 (40.7%)			
Male	143 (42.8%)	101 (53.2%)	16 (59.3%)	vs. Female	1.56 (1.06, 2.31)	**0.025**
Race (n, %)						
African Descent	72 (21.6%)	38 (20.0%)	1 (3.7%)	(Reference)		
Asian Descent	52 (15.6%)	60 (31.6%)	14 (51.9%)	vs. African Descent	2.63 (1.42, 4.88)	**0.002**
European Descent	199 (59.6%)	89 (46.8%)	11 (40.7%)	vs. African Descent	0.93 (0.54, 1.58)	0.784
Other / Not Reported	11 (3.3%)	3 (1.6%)	1 (3.7%)	vs. African Descent	0.67 (0.16, 2.85)	0.589
Spherical Equivalent (D)	−1.51 (−1.84, −1.17)	−1.55 (−1.97, −1.12)	−1.25 (−2.62, 0.13)	per D lower	1.09 (1.02, 1.17)	**0.015**
VF MD (dB)	−4.54 (−5.23, −3.84)	−7.97 (−9.20, −6.74)	−9.91 (−12.99, −6.82)	per dB lower	1.10 (1.07, 1.13)	**<0.001**
IOP (mmHg)	13.8 (13.3, 14.3)	13.0 (12.4, 13.7)	12.3 (9.8, 14.8)	per mmHg higher	0.94 (0.90, 0.99)	**0.013**
AL (mm)	24.7 (24.5, 24.8)	24.9 (24.7, 25.1)	25.4 (24.9, 26.0)	per mm higher	1.36 (1.20, 1.54)	**<0.001**
CCT (μm)	536.7 (531.9, 541.4)	535.2 (529.8, 540.6)	534.5 (524.7, 544.4)	per μm higher	1.00 (0.99, 1.00)	0.445
BMO Ovality Index	0.88 (0.87, 0.89)	0.86 (0.85, 0.87)	0.83 (0.80, 0.87)	per 0.1 lower	1.57 (1.21, 2.04)	**<0.001**
BMO Rotation Angle (°)	33.3 (30.7, 35.9)	31.4 (27.8, 35.0)	25.7 (17.0, 34.3)	per 10 degrees lower	1.07 (0.97, 1.17)	0.159
BMO Tilt Angle (°)	2.2 (1.9, 2.4)	3.1 (2.6, 3.5)	3.5 (2.4, 4.6)	per degree higher	1.24 (1.14, 1.35)	**<0.001**
BMO Area (mm^2)	2.13 (2.06, 2.21)	2.20 (2.11, 2.28)	2.38 (1.96, 2.79)	per 1 mm^2 higher	1.40 (1.03, 1.90)	**0.032**
ΔBMOC (μm)	50.6 (44.4, 56.8)	61.8 (52.9, 70.8)	144.8 (110.3, 179.4)	per 10 mm higher	1.06 (1.03, 1.10)	**<0.001**
OCT Quality Score	29.5 (29.1, 29.9)	29.6 (29.1, 30.2)	28.4 (26.5, 30.3)	per unit lower	0.99 (0.94, 1.04)	0.614
Myopia Group						
*Non-High Myopia (AL ≤ 26mm)	292 (87.4%)	134 (70.5%)	12 (44.4%)			
*High Myopia (AL > 26mm)	42 (12.6%)	56 (29.5%)	15 (55.6%)	vs. No Myopia	3.38 (2.11, 5.42)	**<0.001**
Global MRW (μm)	225.8 (216.5, 235.1)	209.2 (198.8, 219.6)	216.6 (189.4, 243.7)	per 10 μm thinner	1.06 (1.03, 1.09)	**<0.001**
Temporal MRW (μm)	172.8 (165.5, 180.1)	161.9 (153.7, 170.1)	172.4 (152.1, 192.8)	per 10 μm thinner	1.04 (1.01, 1.08)	**0.013**
TS MRW (μm)	209.6 (199.2, 219.9)	187.2 (174.9, 199.6)	204.6 (174.4, 234.8)	per 10 μm thinner	1.04 (1.02, 1.06)	**<0.001**

	BMO Location Status			Univariable Analysis		
	Accurate automated (n = 334)	Manually Corrected (n = 190)	Indiscernible (n = 27)	OR Units	Inaccurate BMO Location OR (95% CI)	p-value
TI MRW (μm)	219.5 (206.4, 232.5)	188.9 (174.9, 202.9)	195.4 (158.6, 232.1)	per 10 μm thinner	1.05 (1.03, 1.07)	**<0.001**
Nasal MRW (μm)	256.9 (246.0, 267.8)	242.2 (229.7, 254.7)	237.0 (201.3, 272.8)	per 10 μm thinner	1.04 (1.02, 1.07)	**<0.001**
NS MRW (μm)	252.1 (240.6, 263.6)	228.2 (214.6, 241.7)	243.4 (205.2, 281.5)	per 10 μm thinner	1.04 (1.02, 1.06)	**<0.001**
NI MRW (μm)	269.0 (255.7, 282.2)	235.2 (219.9, 250.5)	259.3 (219.4, 299.2)	per 10 μm thinner	1.05 (1.03, 1.07)	**<0.001**

*Axial length ≤26mm is defined as non-high myopia and axial length >26mm as high-myopia

Data is presented as mean (95% CI) for continuous variables and count (percentage) for categorical variables.

Significance is determined by logistic generalized estimating equations.

Abbreviations: AL, axial length; BMO, Bruch's membrane opening; IOP, intraocular pressure; MD, mean deviation; NI, nasal inferior; NS, nasal superior, OCT, optical coherence tomography; SE, spherical equivalent; TI, temporal inferior; TS, temporal superior; VF, visual field

Table 4:

4 Multivariable logistic generalized estimating equations models output for predicting inaccurate locations with BMO ovality index, BMO tilt angle, axial length, axial high myopia and spherical equivalent included in separate models.

	Model 1		Model 2		Model 3		Model 4		Model 5	
	Odds Ratio (95% CI)	**p-value**	**Odds Ratio (95% CI)**	**p-value**	**Odds Ratio (95% CI)**	**p-value**	**Odds Ratio (95% CI)**	**p-value**	**Odds Ratio (95% CI)**	**p-value**
Male (vs. Female)	1.17 (0.76, 1.81)	0.469	1.16 (0.75, 1.79)	0.515	1.04 (0.67, 1.62)	0.853	1.09 (0.71, 1.68)	0.690	1.20 (0.77, 1.88)	0.428
Asian Descent (vs. African Descent)	1.72 (0.89, 3.32)	0.107	1.29 (0.65, 2.56)	0.462	1.43 (0.73, 2.81)	0.295	1.31 (0.66, 2.58)	0.441	0.88 (0.40, 1.91)	0.739
European Descent (vs. African Descent)	0.65 (0.36, 1.15)	0.136	0.60 (0.34, 1.06)	0.077	0.57 (0.32, 1.01)	0.053	0.57 (0.32, 1.00)	0.052	0.63 (0.36, 1.09)	0.096
Other Race / Unreported (vs. African Descent)	0.94 (0.20, 4.46)	0.937	0.94 (0.18, 4.90)	0.938	0.90 (0.16, 5.07)	0.905	0.81 (0.14, 4.76)	0.812	1.04 (0.22, 4.87)	0.959
BMO Area (per mm ^{2})	0.94 (0.63, 1.42)	0.783	0.92 (0.60, 1.42)	0.701	0.86 (0.58, 1.29)	0.477	0.88 (0.59, 1.32)	0.529	0.98 (0.65, 1.48)	0.925
BMO Centering (per 10 mm)	1.01 (0.98, 1.05)	0.484	1.01 (0.97, 1.05)	0.691	1.02 (0.98, 1.06)	0.283	1.02 (0.98, 1.06)	0.314	1.04 (1.00, 1.08)	**0.033**
Glaucoma (vs. Healthy)	4.50 (2.50, 8.12)	**<0.001**	4.36 (2.39, 7.96)	**<0.001**	4.39 (2.45, 7.86)	**<0.001**	4.67 (2.60, 8.40)	**<0.001**	3.96 (2.14, 7.32)	**<0.001**
BMO Ovality index (per 0.1 units lower)	1.45 (1.09, 1.93)	**0.010**								
BMO Tilt (per degree)			1.18 (1.07, 1.30)	**0.001**						
Axial Length (per mm)					1.20 (1.02, 1.40)	**0.023**				
Axial High Myopia (Axial Length > 26mm)							2.41 (1.36, 4.25)	**0.002**		
Spherical Equivalent (per D lower)									1.07 (0.98, 1.17)	0.134

Table 5.

Characteristics and factors associated with indiscernible Bruch's Membrane Opening (BMO)

Total number of eyes	**Non-High Myopia (n=438)**	**High Myopia (n=113)**	**Total (n=551)**
Number of eyes with Indiscernible BMO/Total number of eyes n (eyes)	12/438 (2.7%)	15/113 (13.3%)	27/551 (4.9%)
Total number meridians[1] with indiscernible BMO (48 meridians per eye)	307/21024 (1.5%)	503/5424(9.3%)	810/26448 (3.1%)
Eyes with indiscernible BMO	**Non-High Myopia (n=12)**	**High Myopia (n=15)**	**Total (n=27)**
Mean number of indiscernible meridians / Total number of eyes with indiscernible BMO	12.8/48 (26.7%)	16.8/48 (35.0%)	14.8/48 (30.8%)
Mean number of indiscernible B-scans by location			
Temporal	13.0/48 (27.1%)	20.9/48 (43.5%)	17.0/48 (35.4%)
Nasal	12.6/48 (26.3%)	12.6/48 (26.3%)	12.6/48 (26.3%)
Total number of b-scans with blood vessel shadowing/ Total number of indiscernible b-scans	93/307 (30.3%)	106/493 (21.5%)	199/800 (24.9%)
Blood vessel shadowing location			
temporal region	26/93 (28.0%)	33/106 (31.1%)	59/199 (29.6%)
nasal region	67/93 (72.0%)	73/106 (68.9%)	140/199 (70.4%)
Total number of eyes with indiscernible BMO due to poor image quality	2/12 (16.7%)	2/15 (13.3%)	4/27 (14.8%)
Total number of indiscernible eyes with clinically visible peripapillary atrophy (PPA)[2]	6/12 (50.0%)	12/15 (80.0%)	18/27 (66.7%)
PPA location in indiscernible eyes with PPA			
Temporal PPA only	3/6 (50.0%)	6/12 (50.0%)	9/18 (50.0%)
Nasal PPA only	1/6 (16.7%)	0/12 (0%)	1/18 (5.6%)
Temporal and Nasal PPA	2/6 (33.3%)	6/12 (50.0%)	8/18 (44.4%)

[1] There are 2 BMO locations for each of the 24 b-scans

[2] based on review of the optical coherence tomography optic nerve head enface images